

This is a repository copy of *Investigation of the homogeneity of particle suspension*.

White Rose Research Online URL for this paper: https://eprints.whiterose.ac.uk/id/eprint/233190/

Version: Published Version

Article:

Wang, Z. orcid.org/0009-0005-7536-7127, Sanders, C. orcid.org/0000-0002-1068-5774, Al-Asady, R.B. et al. (1 more author) (2024) Investigation of the homogeneity of particle suspension. Chemical Engineering Research and Design, 205. pp. 280-291. ISSN: 0263-8762

https://doi.org/10.1016/j.cherd.2024.03.034

Reuse

This article is distributed under the terms of the Creative Commons Attribution (CC BY) licence. This licence allows you to distribute, remix, tweak, and build upon the work, even commercially, as long as you credit the authors for the original work. More information and the full terms of the licence here: https://creativecommons.org/licenses/

Takedown

If you consider content in White Rose Research Online to be in breach of UK law, please notify us by emailing eprints@whiterose.ac.uk including the URL of the record and the reason for the withdrawal request.



ELSEVIER

Contents lists available at ScienceDirect

Chemical Engineering Research and Design

IChemE

journal homepage: www.elsevier.com/locate/cherd



Investigation of the homogeneity of particle suspension

Zheng Wang a,*, Constantijn Sanders b, Riyadh B. Al-Asady a, Agba D. Salman a

- ^a Department of Chemical and Biological Engineering, University of Sheffield, Mappin Street, Sheffield S1 3JD, UK
- ^b Nestlé Product Technology Centre, Nestlé Strasse 3, Konolfingen CH-3510, Switzerland

ARTICLE INFO

Keywords: Focused Beam Reflectance Measurement (FBRM) Floating particles Suspended particle Sticking particles Settling particles

ABSTRACT

The homogeneity of particle suspension has attracted more attention in the fields of rehydrating milk beverages. This work focus on size characterization of the floating, sticking (on the wall), suspended and settling particles involving both online and offline sizing techniques. Focused Beam Reflectance Measurement (FBRM) is a powerful online technique that is capable for measuring and analysing chord length distribution (CLD) of the suspended particles in liquid. It has been widely used in terms of monitoring size evolution of crystallization and sedimentation processes. In this work, a new approach that involves FBRM probe to measure the particle size distribution has been developed. The probe is placed at three different height levels in a standard container after one hour of free sedimentation. The results suggest that the finest fraction is dominant at all three heights but the percentage of it decreases with an increase of larger particles when looking at the bottom. Besides, all the floating, sticking and settling particles are collected and analysed, and the particle size distributions (PSDs) are obtained and compared using the offline sizing techniques, such as optical microscope and Camsizer. In the results, the suspended particle is the smallest one followed by the sticking and the floating particles, while the settling particle is the largest. However, for the sticking particles sticking on the wall, a great number of agglomerates is found during the test due to adhesion force, indicating that the size distribution might be overestimated. Based on the results, the target particle size range that can be stably suspended in the model suspension was selected by eliminating the unfavourable fractions.

1. Introduction

In still particle suspension, the small particles tend to stay in the liquid, while the big particles may settle down to the bottom. Some particles with different hydrophobicity may float on liquid surface due to capillary force. Inhomogeneity of suspension will trigger several consequences such as irritating esophagus of consumers and reducing bioaccessibility of the nutrients. Fig. 1 surmises the three unfavourable scenarios when suspending solid particle into liquid, such as the floating particle (Particle A), the fine particle sticking on the wall (Particle B) and the settling particle (Particle C). All the particles that cannot be well dispersed into the liquid and will reduce the concentration of the waterinsoluble particles are considered in this work. Particle A, the particle steady floating on the liquid surface, is subject to gravity force (F_{σ}) and buoyancy force (F_B) , as well as capillary force (F_C) when staying on the water surface (the junction of air phase and liquid phase). Bozon et al (Bozon et al., 2022), investigated the effects of particle hydrophobicity on floating phenomenon. Coconut oil was coated on acid treated glass beads as the model material and capillary force is defined in the

following equation.

$$F_c = 2\pi R_p \gamma \quad \sin\alpha \quad \sin\beta \tag{1}$$

where $R_{\rm p}$ is particle radius, γ is liquid surface tension, α and β are immersion angle and meniscus slope angle respectively. The capillary force is positively relevant to particle size.

When a solid particle moving in liquid medium (Particle C and D, settling particles and suspended particles), drag force will act on the particle opposite to the relative velocity (Zhang et al., 2023; Kriebitzsch et al., 2013; Laxminarsimha Rao and Das, 2015; Gao et al., 2022). When drag force (F_D) increases with the increase of particle settling velocity and is equal to gravitational force (F_g) minus buoyancy force), the particle will reach to the terminal speed, where these forces in a steady laminar flow are defined (Laxminarsimha Rao and Das, 2015)

$$F_g = F_D = (\rho_s - \rho_l)gV = 3\pi\mu W_s d \tag{2}$$

where g is the acceleration attributed by gravity; ρ_s and ρ_l are the densities of the particle and liquid; μ is dynamic viscosity of liquid; V is the particle volume; d is the particle diameter; and W_s is particle terminal

E-mail address: zwang329@sheffield.ac.uk (Z. Wang).

^{*} Corresponding author.

LIST o	of symbols
D	Mean diameter of particles [m]
h	Height of liquid level [m]
r	Radius of capillary [°C]
R	Liquid wetting area [m ²]
T	Total time duration of droplet penetration [s]
V_0	Droplet volume [m ³]
$\theta_{ m d}$	Dynamic contact angle [°]
μ	Viscosity of the liquid [Pa·s]
γLV	Surface tension of the liquid [mN/m]
φ	Porosity of the powder bed [-]

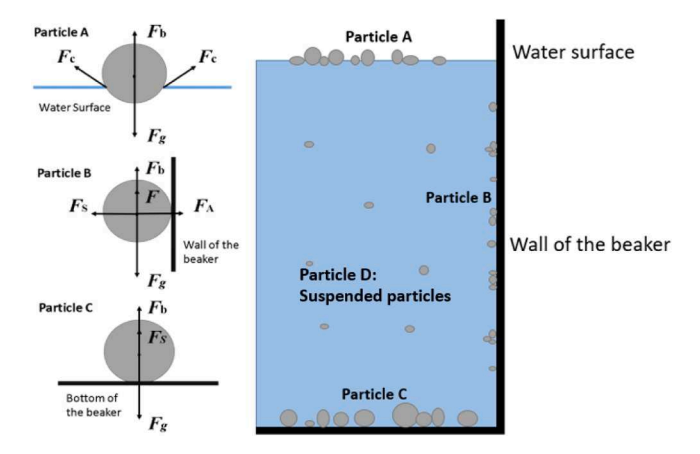


Fig. 1. The problem faced when suspending solid particles into liquid. Particle is floating on the liquid surface. Particle B is sticking on the wall of the beaker. While particle C settles down to the bottom, where F_g is gravity force, F_B is buoyancy force, F_c is capillary force, F_A is adhesion force and F_D is drag force.

velocity. Substituting V by $1/6\pi d^3$ by assuming a spherical particle and reorganizing Eq. (2), Eq. (3) is derived as followed

$$d^2 = \frac{18}{g} \frac{\mu w_s}{\rho_s - \rho_l} \tag{3}$$

This equation reveals the relationships between particle diameter, particle relative velocity and solid to liquid density in the system where particles steady settle down in a laminar flow.

The resisting effects on settling velocity in a system that contains particles with multiple size ranges are more complicated (Krishnamoorthy, 2010). That is because the settling velocity of each particle will be affect by the counter flow of the displaced fluid that caused by the movement of other particles (Govier et al., 1973). This effect is largely depended on particle concentration of the mixture. The complexity counter flow or particle collision make it hard to precisely predict the particle size distribution in suspension using the theoretical models. It is reported in the experimental work that during sedimentation process, four different zones were observed (Krishnamoorthy, 2010). Starting at the highest level, the system is composed of four parts: (1) a clear and transparent liquid region with a small amount of the finest particles suspended inside, (2) a settling zone at the top where small particles settle, (3) a settling zone at the bottom where both particles with different size are present, and (4) a layer of sediment at the bottom of the system. As time developed, the final mixture contains only clear liquid, and the deposit.

Apart from the floating and settling particles, it has been found that a small amount of fine particles (Particle B) tends to stick to the wall of the container due to the adhesion force (F_A) . The adhesion force in air is

fully investigated, which largely depends on a variety of material properties, including particle size (Felicetti et al., 2009) and surface roughness (Götzinger and Peukert, 2004). But limited number of papers of work focus on the sticking particles on a surface inside liquid. Negreiros et al (Negreiros et al., 2015). measured the adhesion force between glass bead and glass surface in static purified sunflower oil using an atomic force microscope (AFM) and compared the results with the calculated van der waals force. The calculated force is larger than the measured value. The sticking particles on the vertical surface (shown in Fig. 1 Particle B) is more complex due to the existence of balance on the particles, involving the gravity force, buoyancy force, friction force and drag effect of the local liquid flow. In this work, sticking particles are visualized and particle size is analysed using the different techniques.

In the clear zone of a suspension after full sedimentation, there are two main regimes on the suspended particles (Particle D), Brownian motion and natural convection. The pure diffusion model, Stokes–Einstein–Sutherland equation, was published and modified to describe the random displacement in two dimensions of a small particle driven by bombardment of surrounding liquid molecules (Bian et al., 2016). However, Brownian motion of the microscale or nanoscale particles in bulk liquid could only be observed under the ideal conditions where rigidly there is no heat transfer between the liquid and the ambient environment or any other types of liquid movement. Otherwise, the liquid will move with particles due to the change of its density with varying temperature, which is called buoyancy flow or natural convection (Murshed et al., 2020; Hagiwara et al., 2014).

Focused Beam Reflectance Measurement (FBRM) is a method that is capable for measuring the chord length distribution (CLD) online. It has been widely used in the fields of crystallization, precipitation and granulation (Sodhi et al., 2019; Kumar et al., 2013). The in situ changes of size profile inside the system are able to be monitored by involving FBRM. One of the advantages is that there is no need to capture the sample from the system or external circulation which might be hazardous and unrepresentative. Compared with other scanning methods, turbidimetry for example, FBRM is capable of measuring counts of particles and particle size distribution within a large range, e.g. from 1 μm to approximately 4000 μm, while turbidimetry only focus on turbidity of the suspension related to particle concentration. Also other online scanning methods are usually applied to the media of high concentration and have higher sensitivity to the background noise. While in a dilute suspension used in the study, FBRM has better stability and anti-interference performance due to its shorter and more focused laser path. Therefore, this technology has been widely used in the field where liquid medium interacts with solid particles and especially involving particle size change during the time. Many parameters are reported to have profound influence on the results. Alex et al (Heath et al., 2002). conclude the effects of the types of model materials on the particle size by reviewing the results from others work. Pual and Brain (Barrett and Glennon, 1999) find the scale of the beaker has no effect on the results but the orientation and position of the probe can heavily affect the counts of particles. Kaushalkumar et al (Dave et al., 2018). also give the similar conclusion. When increasing the probe angle or moving the probe to the centre, the counts of particles will increase. In this work, all parameters are fixed and three different techniques of size measurement are involved and both online and offline techniques are compared.

The objective of this work is to investigate the boundaries on particle size between the particles at different locations in calcium carbonate suspension, including floating, sticking, settling and suspended particles, and select the target size range that can be stably suspended in the model suspension. To achieve that, both online and offline sizing techniques are involved and evaluated. Meanwhile, standard glass beads are used to compare the difference between the three involved sizing techniques. And the suspensions are kept for 7 days to study the particle size change in a long period.

Table 1Particle size of the powders.

	D ₁₀ (μm)	D ₅₀ (μm)	D ₉₀ (μm)
CaCO ₃ (Kirsch Pharma)	2.7	5.3	7.9
CaCO ₃ (Longcliffe)	4.7	16.5	77.7

2. Materials and methods

Two types of calcium carbonate from Longcliffe Quarries Ltd, UK and Kirsch Pharma GmbH, Germany are used as the model material. The size distribution of the model material is measured using Camsizer X-Dry (Retsch, Haan, Germany) and the results are shown in Table 1.

The powder from Kirsch Pharma has comparably lower size distribution. The D_{90} of the Kirsch's powder is lower than 10 μ m. The true density of calcium carbonate was provided by the supplier of 2.7 g/cm³.

2.1. Sessile drop goniometry

In order to explain particle floating phenomenon, hydrophobicity of two powders is compared. The powders are sieved before compression using a 13 μm sieve (Retsch, Haan, Germany) to reduce the influence of particle size. Each powder is precisely weighted 10 g. Universal Testing Machine (Instron, Norwood, US and Anton Paar, Graz, Austria) is used to prepare tablets under the fixed compress pressure at 45 KN (64 MPa). The diameter of the die is 30 mm. The resultant tablets are weak and easy to break but with smooth surface. The tablets were carefully collected and handled for sessile drop goniometry.

The derivation of penetration time and appearance contact angle of droplet wetting powder bed is given as followed. The Washburn equations describe the rate (dh/dt) and height (h) of a liquid rise into a capillary tube with radius (r) (Denesuk et al., 1993).

$$\frac{dh}{dt} = \sqrt{\frac{r\gamma_{LV}\cos\theta_d}{8\mu t}}\tag{4}$$

where θ_d is the dynamic contact angle. μ and γ_{LV} are the adhesive viscosity and surface tension.

The capillary radius in a powder is difficult to be directly measured, but can be estimated by the powder bed porosity (φ), surface area, material density, and mean particle diameter (d) of a powder (Bai et al., 2019).

$$r = \frac{d\varphi}{3(1-\varphi)} \tag{5}$$

Further models simplify the powder surface as a solid consisting of a number of parallel capillaries. The flow rate of liquid penetrating powder (dV/dt) can be expressed as the following equation, where R is the liquid wetting area (Denesuk et al., 1993):

$$\frac{dV}{dt} = \pi R^2 \varphi \frac{dh}{dt} \tag{6}$$

Substituting the Washburn equation (Eq. (4)) into the flow rate expression (Eq. (6)) and integrating over time (t) establishes the expression for the total time duration of droplet penetration (T). The dynamic contact angle in capillaries can be expressed as the following equation:

$$\cos\theta_d = \frac{24V_0^2(1-\varphi)\mu}{\gamma_{LV}\pi^2R^4\varphi^3dT}$$
 (7)

where d is estimated as D_{50} , and V_0 is the droplet volume. V_0 is volume of droplet obtained by counting the number of droplets in 5 mL. 3 replicates were made. The tablet porosity is measured in the following part and calculated by $\varphi = (V_{\rm Envelope} - V_{\rm Skeletal}) / V_{\rm Envelope}$ (Denesuk et al., 1993), where $V_{\rm Envelope}$ is the physical volume of the tablet calculated by

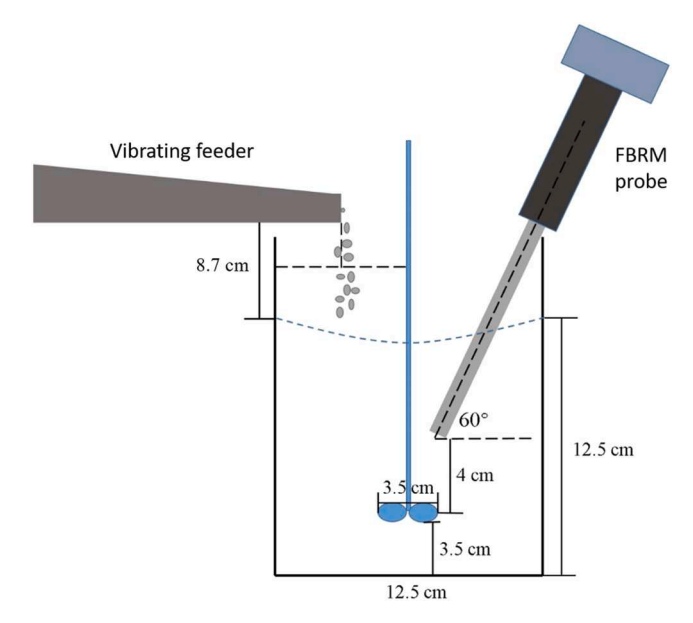


Fig. 2. Schematic of sedimentation rig.

its physical dimensions and $V_{\rm Skeletal}$ is estimated by the true density of CaCO₃ and the mass.

2.2. Tablet actual porosity

The tablet actual porosity is measured before sessile drop goniometry using X-Ray tomography (MicroCT 35, Scanco Medical AG, Bruettisllen, Switzerland). The maximum resolution of the scan is 3 μm and each tablet has been scanned for 60 slides. The tablet actual porosity is defined as the area ratio of solid and air based on the grey value.

2.3. Characterization of floating, sticking and settling particles

In order to investigate the size distribution of particles at different location, samples are collected and tested. 25 g of Longcliffe's calcium carbonate powder is mixed with 1000 mL deionized water with 30 min of agitation. The impeller speed is kept constant at 500 rpm. The suspension is placed in the lab at room temperature (22 \pm 0.5 $^{\circ}$ C) for 1 h of free sedimentation.

Firstly, the floating particles are gently collected using a spoon. The floating particles are move to an empty beaker and then dispersed and diluted by deionized water. After removing all floating particles, the particle suspension is transferred to a new beaker by a large syringe. The particles staying on the wall are wiped out and collected using a customised tool. The tool with sticking particles is moved to a beaker and the particles are washed out by a stream of deionized water. The samples from different parts are measured using Camsizer (X-Flow, Retsch, Haan, Germany). Lastly, the particles at the bottom are dry using a hot plate and the dried sediments are gently crushed. The size of deposit is tested using Camsizer with different module, X-Dry, because X-Flow is only capable of measuring the particles well-dispersed in the liquid. Samples were clearly labelled and tested three times.

2.4. Focused beam reflectance measurement (FBRM)

The size of suspended particles after 1 h of free sedimentation at three different heights is measured by FBRM. The experimental settings are described as follow. Fig. 2 shows the locations of FBRM probe (Particle Track G600Ex, Mettler Toledo, USA), vibratory feeder and the agitator and the dimensions of the beaker and impeller. The diameter of the impeller blade is 3.5 cm which is equals to the off-bottom distance of the impeller. The inner diameter of the beaker is 3.6 times of the

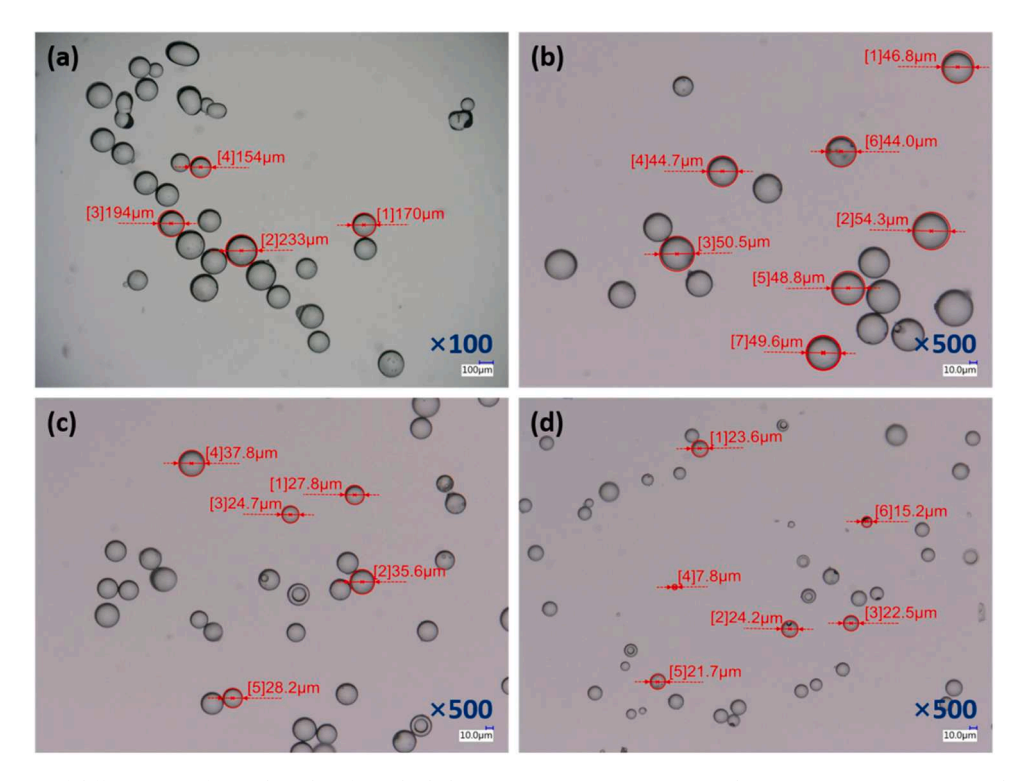


Fig. 3. Pictures of different size of particles taken from the light microscope. (a) 106-250 µm, (b) 45-63 µm, (c) 25-45 µm and (d) <25 µm.

impeller. And the liquid height is 12.5 cm without adding the powder. The dimensions could be referred to ref (Mitchell et al., 2020).

The vibratory feeder is placed above the vessel such that particles are dropped from a height of 8.7 cm above the still liquid surface, and the feeder is positioned tangentially such that particles contact the water halfway between the impeller shaft and the vessel wall (the centre of this stream is positioned at the half-way point). The feed rate is fixed and measured at 1.67 g/s. The FBRM probe, shown in Fig. 2, is inserted inside the liquid directly nearby the shaft of the impeller and is positioned 4 cm above the rotating blades with an angle of 60° . According to the user manual of Mettler Toledo Particle Track G600Ex, it is recommended that the probe should be inserted at an optimal angle (45° to 60°) relative to the process flow. In this work, the shape of the beaker impedes the probe approaching the angle of 45° , so 60° is applied instead.

The FBRM probe was cleaned every 10 min during the test and inserted back to the same position due to the particles cumulatively sticking on the window of the probe. During cleaning, the probe was washed by deionized water and wiped using lens tissue until the total count of particle in pure water reduced to 10 or below.

The suspension was prepared in room temperature 1 h before the measurement. Totally 37.5 g of calcium carbonate powder was weighted and mixed with 1500 mL distilled water using an impeller (Lightnin A100, Rochester, NY, USA) running constantly at 500 rpm for 30 min. The impeller was taken out after agitation. And the suspension was placed in room temperature for 1 h sedimentation before the measurement starts. The probe was then placed at different heights in the liquid with the same angle of 60° (top, middle and bottom, 1.5 cm, 6.0 cm and 10.5 cm respectively) in order to monitor the change of size distributions at different heights.

Static size measurement suspended particles for a long period using light microscopyThe CaCO₃ particles were suspended in distilled water, specifically, 5 g of powder in 200 mL liquid. Suspensions were agitated by using a magnetic stirring hotplate (Dragon Lab, MS7-H550-Pro, China) for 30 min with the same rotating speed (500 rpm). Samples were obtained after 1–7 days of sedimentation individually at the room temperature. Small amount of colloid was gently taken following the

order of the top, middle and bottom (6.5 cm, 4 cm and 1.5 cm from the deposit) by using a syringe with a rubber pipe on its tip. Sample was placed on glass slide and heated to accelerate evaporation of water. The dried particles were observed under the Light Microscopy (Keyence, Osaka, Japan).

The software (VHX application, Keyence, Osaka, Japan) was involved to calculate the diameter of the particles based on area. More than ten pictures were captured under $\times 1000$ magnification from each sample to acquire enough amount of particles for the particle size analysis. Totally more than 3000 particles were involved for each sample. Diameters (d) of particle were equivalent to the circle with the same projection area (A), which was determined by $A=\pi d^2/4$. Next the data is divided into 25 intervals with a step of 0.5 micron based on the calculated d, such as $1.0-1.5~\mu m$, $1.5-2.0~\mu m$ $2.0-2.5~\mu m$ and so on. Then the counts of particles inside each interval were simply counted and converted to percentage.

2.5. Comparison of the three sizing techniques

In order to indicate the difference of the size distributions measured by the three involved sizing techniques. The standard glass beads are used in this part because of its regular shape and smooth surface to reduce the risk of error. The three involved sizing techniques in the work are compared and evaluated. The glass beads were separated into four different size classes, $<25~\mu m$, $25-45~\mu m$, $45-63~\mu m$ and $106-250~\mu m$. All classes of glass beads were observed and measured under light microscope, two Camsizer modules (X-flow and X-dry) and FBRM with three replicates. Totally, 16~groups of data are obtained.

3. Results and discussion

3.1. Comparison of sizing techniques

Fig. 3 shows the pictures obtained by the light microscope. As the results, the glass beads are spherical. The size of particles measured by the microscope is generally synchronous with screen apertures. Few particles with size smaller than $45 \, \mu m$ did not pass through the sieve

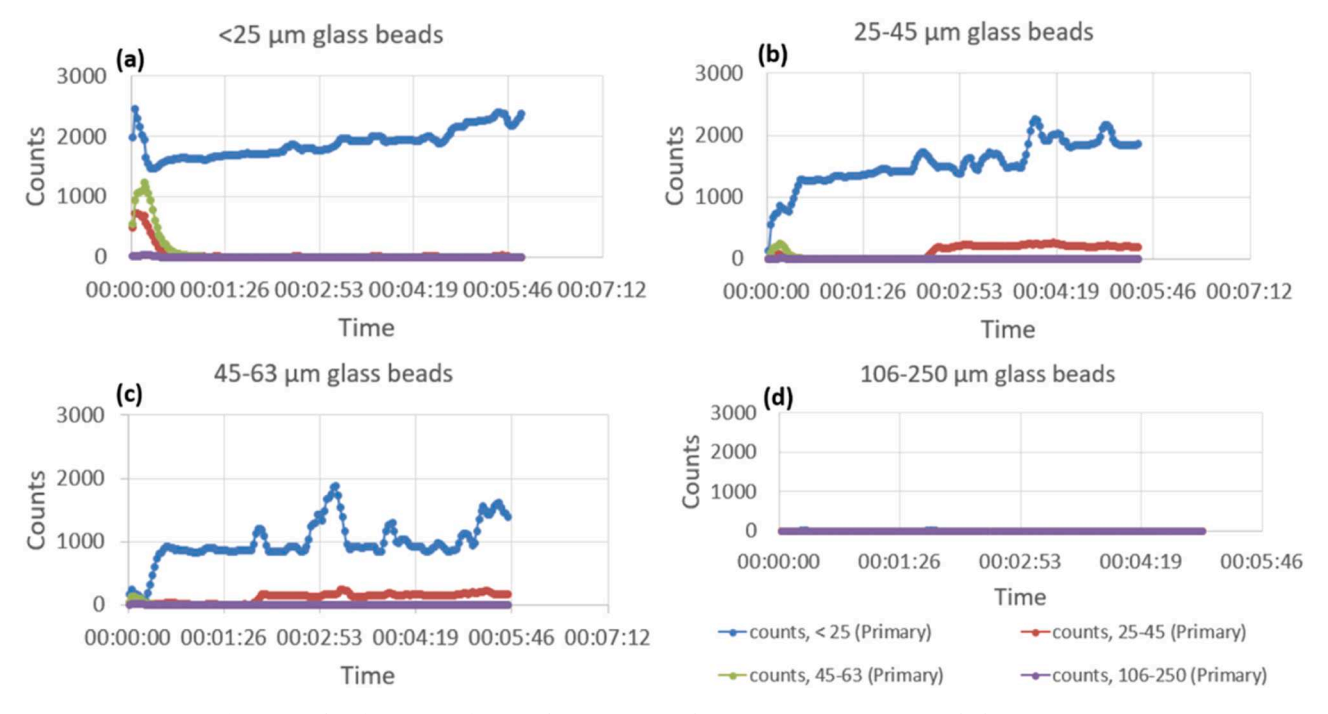


Fig. 4. Results of FBRM test for particles (a) $<25~\mu m$, (b) $25-45~\mu m$, (c) $45-63~\mu m$ and (d) $106-250~\mu m$.

10

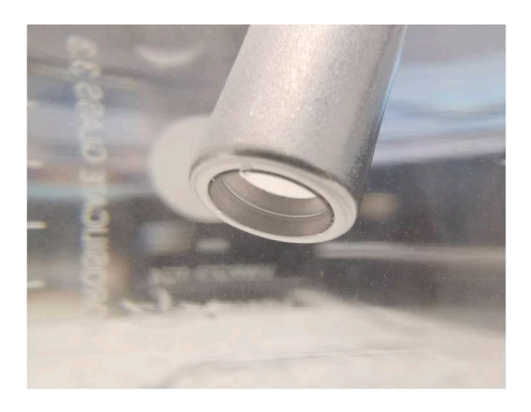


Fig. 5. Picture of the probe during measurement. Lots of particles accumulate on the arm of the probe.

8 d3 [%] 6 2 0 n 10 20 30 40 50 60 70 80 Size [um] —1-25 μm —25-45 μm —45-65 μm —106-250 μm

X-fow

45 um

63 um

25 um

Fig. 6. Size distribution measured by X-flow using different size of glass beads, where the y-axis q3[%] is the distribution frequency in small intervals and x-axis is particle size (same below).

screen. That might due to the strong Van Der Waals and electrostatic forces within dry fine particles, which make the powder bed cohesive and hinder the particles passing through the screen (Castellanos, 2005).

After sieving, 2 g of glass beads in four size classes (106–250 $\mu m,\,45–63~\mu m,\,25–45~\mu m$ and $<\!25~\mu m$) was mixed with 200 mL deionised water separately and agitated by magnetic stir for 10 min. The probe is directly inserted in the middle of the suspension at time 0. Four suspensions were prepared and tested using different samples (different size class of glass beads). The results are as followed.

For the biggest particles (Fig. 4d), no particle could be detected due to the very fast settling process. When looking at the smaller particle, $45–63~\mu m$ (Fig. 4c), the $<25~\mu m$ particles are suspended in liquid with only small amount of $25–45~\mu m$ particles. The similar phenomenon also can be observed in Fig. 4b. Because FBRM can measure the chord length distribution, random chord could vary from 0 to the diameter of the particle (maximum). So the count of $<25~\mu m$ particles inevitably includes some of larger particles. That would explain the existence of small particles in both $25–45~\mu m$ and $45–63~\mu m$ samples. One possible reason of the great fluctuation in Figs. 4b and 4c could be the collapsing particles from the probe. During sedimentation, some particles began to accumulate on the probe (shown in Fig. 5). Sometime the particles

collapsed and detached from the probe and settled down. The signals would fluctuate when the particles passed through the window. According to the results, the collapse is more serious in the group of $45{-}63~\mu m$, compared with the smaller groups, showing the balance of attaching forces and gravity force.

There is a clear trend that when decreasing the sample size, the number of small particles ($<25\,\mu m$) increase, from 1000 to 1500 in Fig. 4c to 1500–3000 in Fig. 4b. That is because the proportion of the small particles increase in the sample after sieving. In Figs. 4a and 4b, the count of $<25\,\mu m$ particle increase with time. Base on picture taken during the test, particle tend to stick and accumulate on the probe.

The glass beads with different size classes ($<\!25\,\mu m,\ 25\text{--}45\,\mu m,\ 45\text{--}63\,\mu m,\ 106\text{--}250\,\mu m)$ are measured using Camsizer with two different modules. For the X-flow, the sample needs to be mixed with water using a magnetic stir (2 g glass beads in 200 mL). The stir rate is 200 rpm and the agitation last 10 min. The sample suspensions were dispersed, agitated and debubbled before test with ultrasonic. The results of X-flow are as follow.

Fig. 6 shows a clear trend that the curve moves to the right when the sample size increase, where q3(x) is defined as q3(x) = dQ3(x)/dx, the

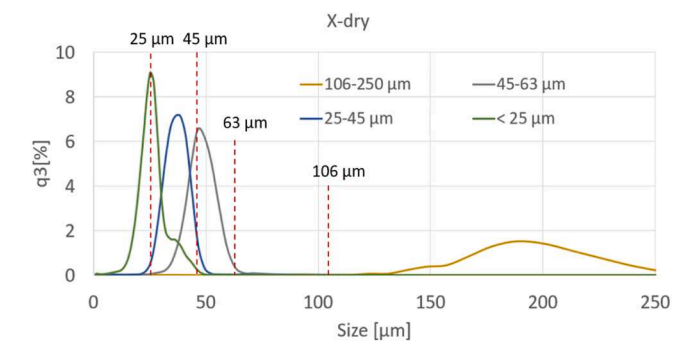


Fig. 7. Size distribution measured by X-dry using different size of glass beads.

frequency distribution based on volume and the first derivative of the cumulative distribution Q3(x). The curve become a straight line overlapping with x-axis regarding of the largest particles. One of the obvious features of X-flow measurement is that it is not able to detect the particles over 55 μm according to Fig. 6 due to sedimentation in the sample barrel.

Besides, compared with the results of FBRM regarding to small particles (Fig. 4a), X-flow shows a great number of particles over 25 μ m, which is not shown in FBRM's results.

The size distribution measured by X-dry are shown in Fig. 7. The trend is the same, but it shows a clear distribution of big particles ($106-250 \mu m$).

Fig. 8 shows comparison based on different size ranges. For the particle $<\!25\,\mu m$ and $25\text{--}45\,\mu m$, X-dry (orange) shows a smaller size distribution than X-flow (flow). While X-dry shows a wider and bigger size distribution in the range of $45\text{--}63\,\mu m$.

3.2. Dynamic contact angle

In order to test the hypothesis that the particles float on the liquid surface is because of its hydrophobicity, a comparison was made using two calcium carbonate powders from different suppliers. No floating particles could be observed in the Kirsch Pharma's powder.

The penetration times of a droplet on the tablet surface were recorded instead of contact angle because water droplets penetrate quickly on the tablet surface, and contact angles change over time. Six replications were made for each material. And the mean penetration times are shown

in Table 3. The calculated contact angle was obtained by Eq. (7) in the content. V_0 and R were measured by experiment. d is estimated by D_{50} of the primary powder. μ and $\gamma_{\rm LV}$ in 20°C were taken as 1 mPa's (Likhachev, 2003) and 72.86 mN/m (Pellicer et al., 2002). Tablet porosity (φ) is measured by X-Ray tomography, where Longcliffe's tablet more porous than Kirsch's tablet.

Table 2 Particle size distributions.

	D_{10} (μm)	D_{50} (μ m)	D ₉₀ (μm)
Suspended Particles	2.6 ± 0.1	$\textbf{4.4} \pm \textbf{0.2}$	7.6 ± 1.5
Sticking Particles	3.7 ± 0.0	7.7 ± 0.2	18.6 ± 1.0
Floating Particles	5.2 ± 0.1	12.0 ± 0.2	24.9 ± 0.3
Settling Particles	5.1 ± 0.3	21.9 ± 1.8	99.0 ± 14.7
Raw material	$\textbf{4.7} \pm \textbf{0.0}$	16.5 ± 0.2	77.7 ± 3.3

Table 3 Penetration time for each tablets.

	Penetration time for tablet under 45 KN	Calculated contact angle, $\cos\theta_{\rm d}$	Porosity of the tablet (area of air/total area)
Longcliffe	$\begin{array}{c} 2.95 \pm 0.17 \ s \\ 1.23 \pm 0.32 \ s \end{array}$	0.12	0.33
Kirsch		0.72	0.21

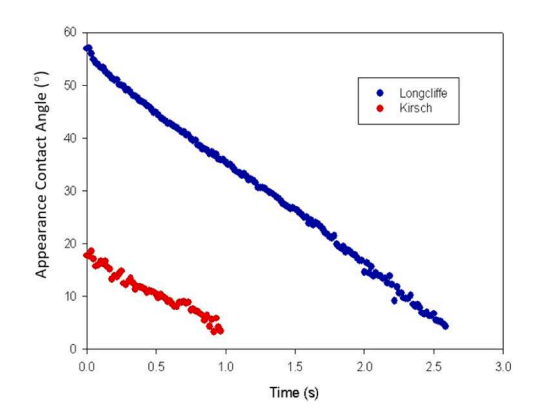


Fig. 9. The contact angle changing with time for 64 MPa tablets.

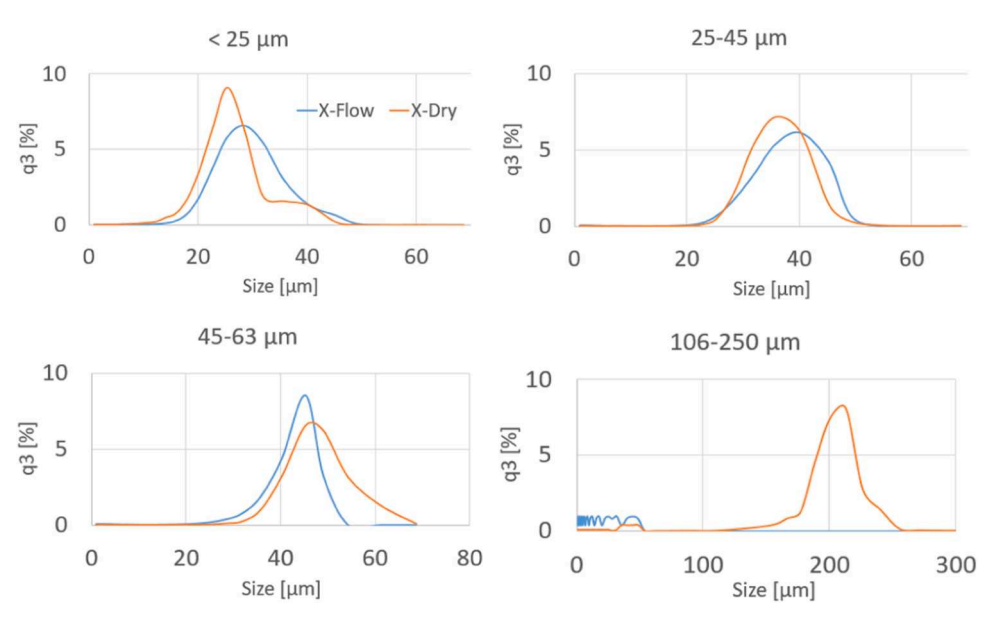


Fig. 8. Comparison of X-flow and X-dry with different size ranges. The orange curve shows results of X-Dry, while the blue shows X-Flow's results.

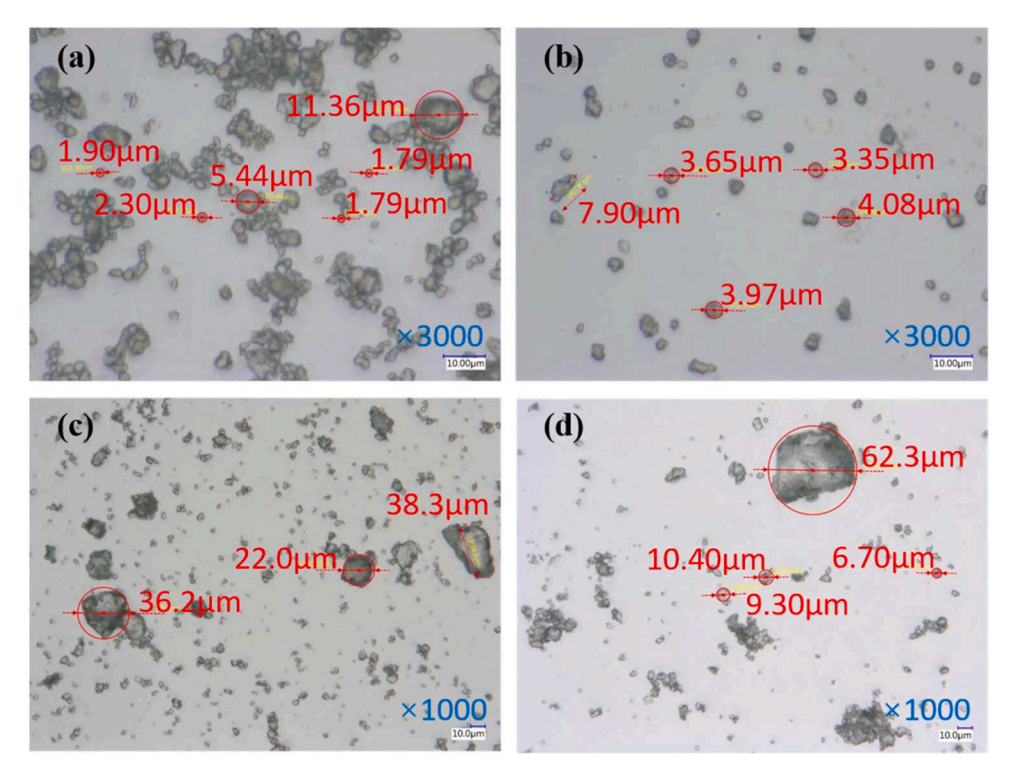


Fig. 10. Pictures taken by Microscope for the particles from different places. (a) and (b) taken under 3000 magnification show the sticking particles and suspended particles respectively. (c) and (d) taken under 1000 magnification show the floating particles and particles from sediments.

Fig. 9 shows the appearance contact angle changing with time for 45 KN tablets, where the blue dot line is $CaCO_3$ from Longcliffe and the red dot line is $CaCO_3$ from Kirsch. It shows a clear difference of the two materials. From the beginning at time 0, the appearance contacts angles are 57° and 18° respectively. Both the appearance contact angle at time 0 and the penetration times show the $CaCO_3$ from Longcliffe is more hydrophobic. According to the suppliers, Longliffe's powder are made from rocks and Kirsch's powder is from crystallization. Longliffe's powder contains more hydrophobic impurities, such as $MgCO_3$ 0.3%, SiO_2 0.3%, Al_2O_3 0.2% and other unknown 0.2%.

3.3. Size distribution of floating, sticking and settling particles

Table 2 shows the cumulative particle size distribution measured by Camsizer. As a results, the particles suspended in the liquid are the smallest among these four followed by the sticking particles collected on the wall. The intermediate particles with hydrophobic surface float on liquid surface. And the largest particles tend to settle down at the bottom. The standard deviation (σ) is calculated by Eq.(8) and shown in Table 2.

$$\sigma = \sqrt{\frac{\sum_{1}^{n} (x_i - \overline{x})^2}{n}} \tag{8}$$

From the pictures shown in Fig. 10, the clear trend on particle size from different samples is visualised. Figs. 10a and 10b display the pictures from the particle sticking on the wall and particles being suspended in the liquid both under 3000 magnification. The fine of sticking particles tend to stick together and form agglomerates in Fig. 10a. And according to the picture, the size of individual particle is comparably smaller than the suspended particles. It indicates the overestimation from Camsier. For the floating particles (Fig. 10c), the particle size reaches to 38.3 μm , which is larger than the sticking and suspended particles but smaller than the settling particles. The largest particle appears in the sediments in Fig. 10d where gravity is dominant.

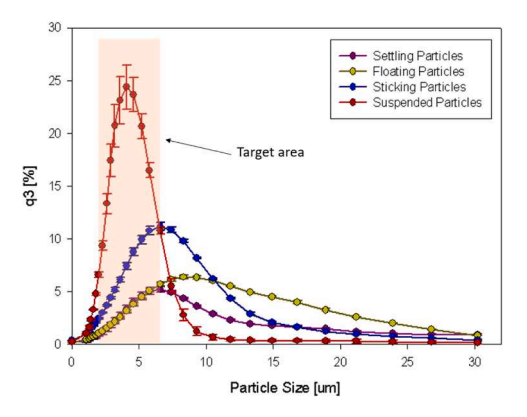


Fig. 11. Size distributions of different part of particles.

Fig. 11 show the particle size distribution based on frequency. The red curve on the left is the particles suspended in the liquid and the curve starts to go down at around 5 μm . Within the range of 0–7 μm , the amount of all particles increase but the suspended particles are dominant. The red curve and the blue curve intersect at around 7 μm . However, according to the pictures from microscope (Fig. 10a), the 1–2 μm particles tend to stick together and form bigger agglomerates. So it might be useful to eliminate the finest fraction of 1–2 μm , through which the target size range of suspended particle could be 2–7 μm , where the unfavourable particles would be removed. The results show a possibility to reduce the particles sticking on the wall, settling down to the bottom and even floating on the surface by simply controlling the particle size.

The adhesion force in air is fully investigated, which largely depends on a variety of material properties, including both the surface and particle material types, particle size, particle charge and surface structure and roughness (Felicetti et al., 2009; Götzinger and Peukert, 2004; Negreiros et al., 2015). But limited study focus on the sticking particles on a surface inside liquid because the scenario changes a lot. Mechanical

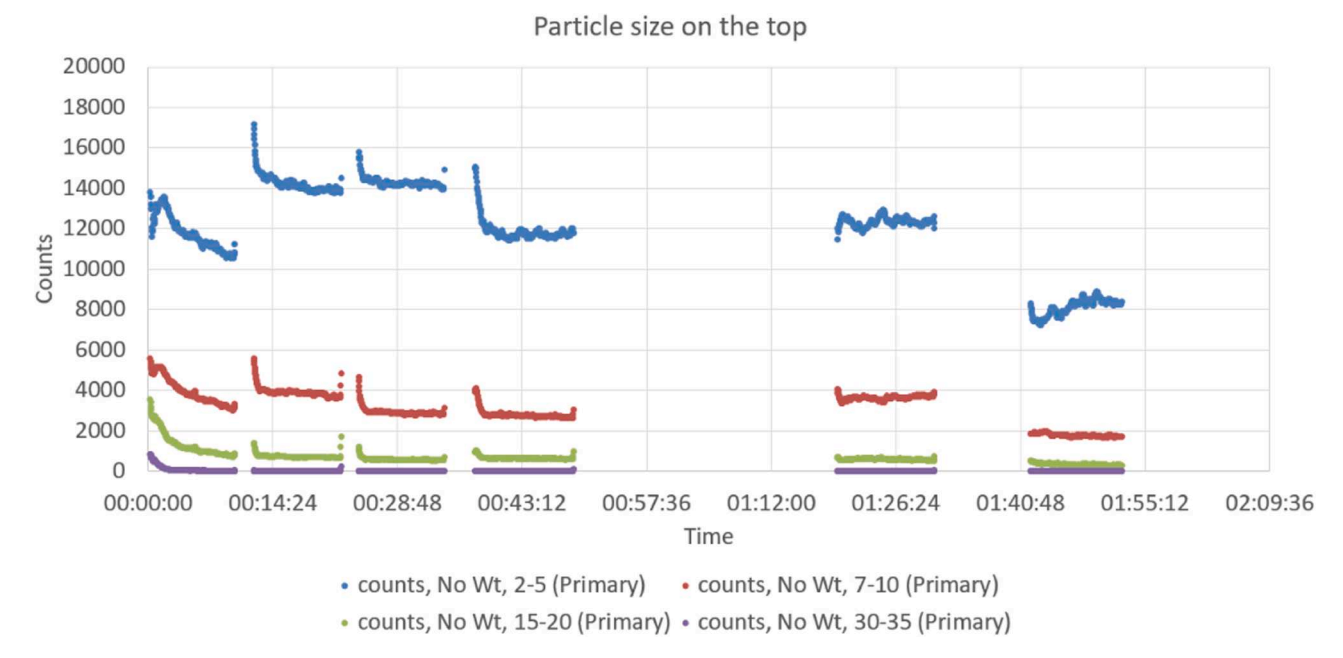


Fig. 12. Results of FBRM based on counts at the top within 2 h. The x-axis is time and y-axis is the counts of particle in a certain size range.

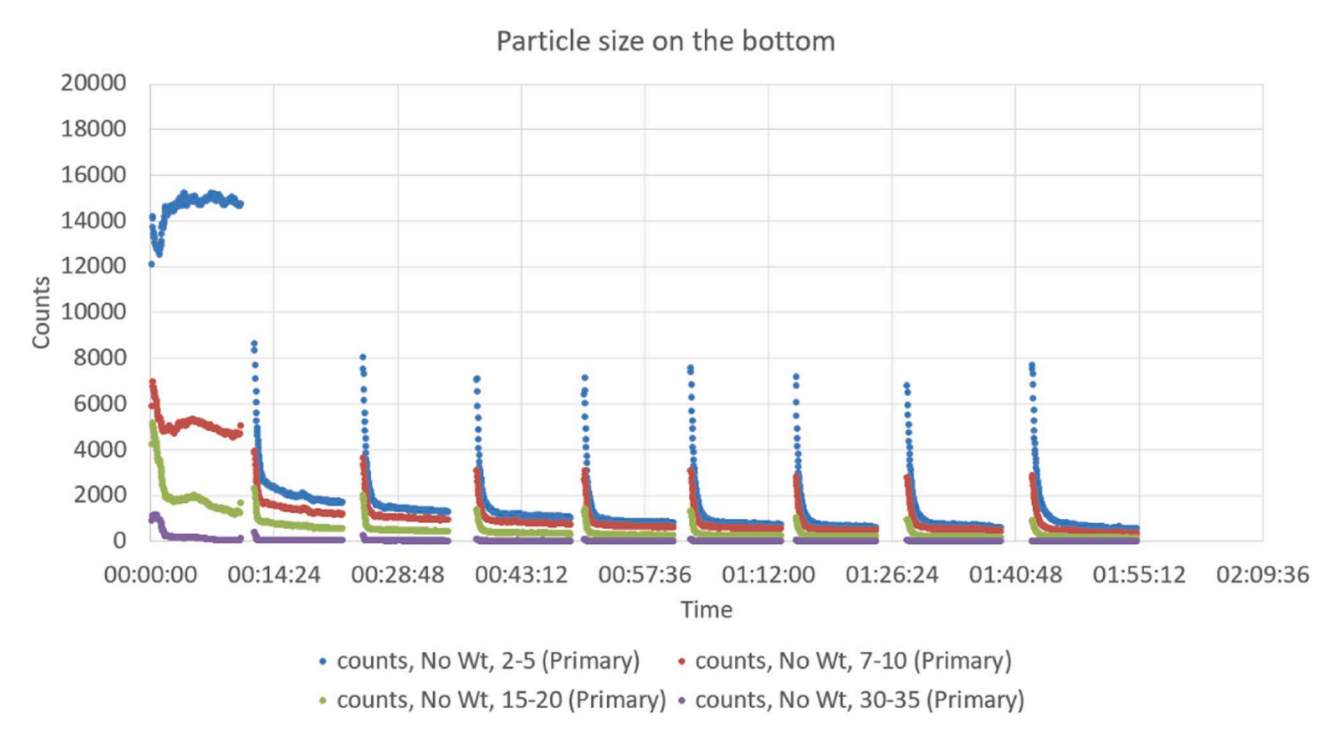


Fig. 13. Results of FBRM based on counts at the bottom within $2\ h.$

force (surface structure interlock), electrostatic force (charging), Van Der Waals force and capillary force if with bubble might be applied on the particles. In this study, we only consider the size range of calcium carbonate particles sticking on the glass wall of the beaker. The interactions between model particles and different types of solid surfaces in pure water could be investigated.

3.4. Results from FBRM

FBRM was used in this part to show the difference of particle size distribution at different heights. The results of the measurements at the top and the bottom heights are shown in Figs. 12–13, where the x-axis is

time and y-axis is the counts of particle in a certain size range. The variation of counts of particles between measurements in one run is large. For example, in Fig. 12, the count of 2–5 μm particles vary between 8000 and 18000 under the same condition. And the counts generally go down during the measurement. At bottom (Fig. 13), the number of counts quickly soared up to 15000 but decreased in the following 10 min and became stable at a low level. The number went up and down irregularly in Fig. 14. However, it shows the same trend and order of counts in different size range between measurements. The count of 2–5 μm particles (blue line) is always the highest among the four size classes regardless of changing in heights in all measurements. And the counts of particles decrease with increase of particle size.

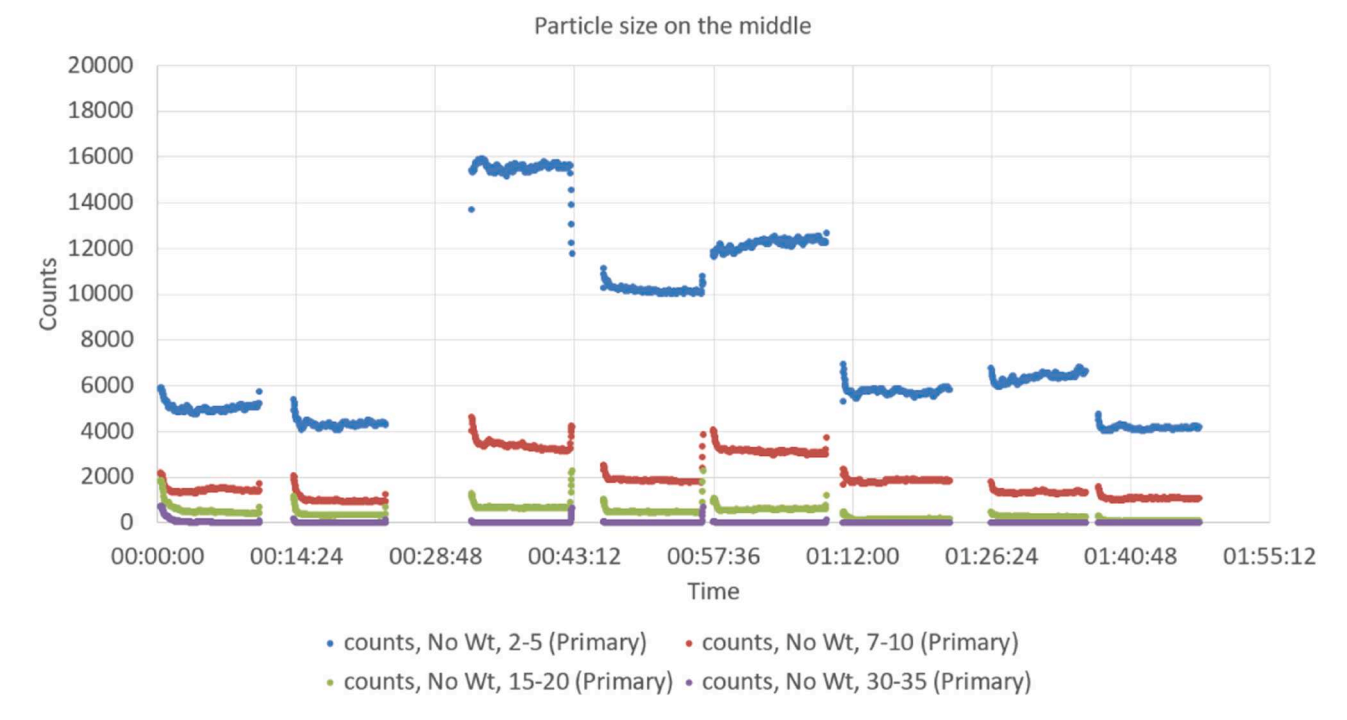


Fig. 14. Results of FBRM based on counts at the middle within 2 h.

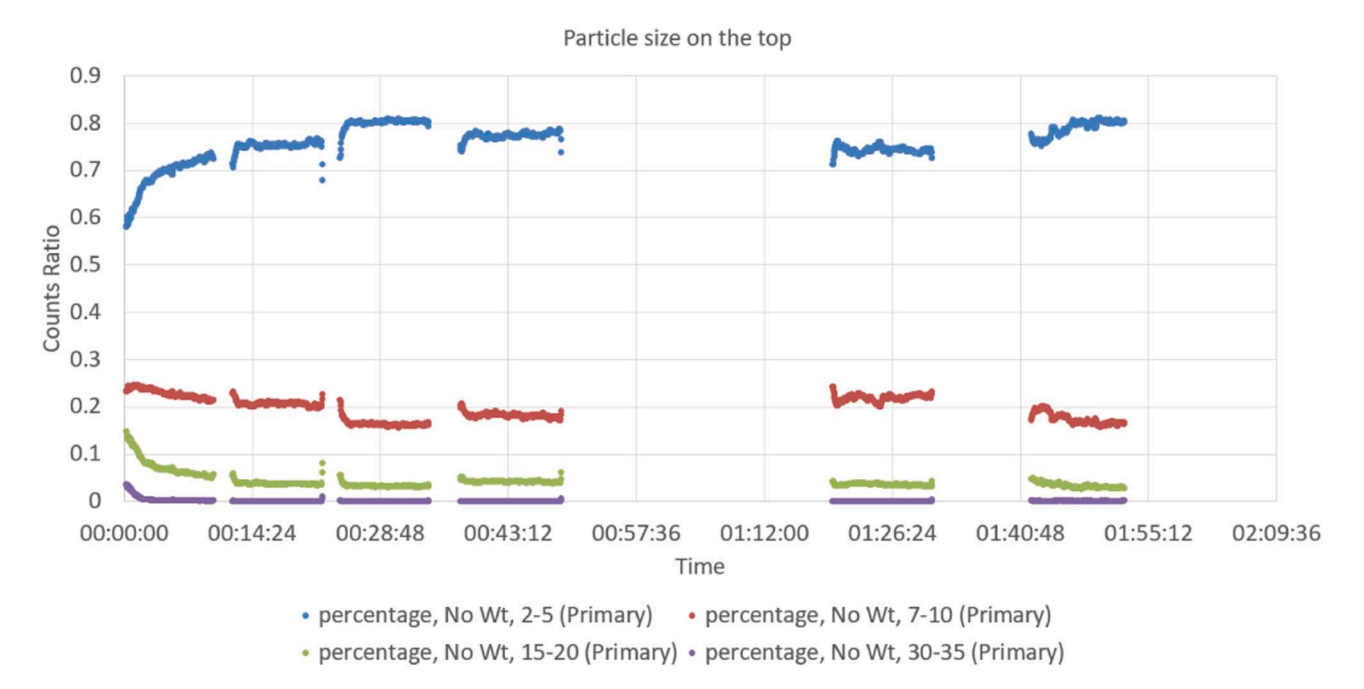


Fig. 15. Results of FBRM based on ratio at the top within 2 h. The x-axis is time and y-axis is the ratio or percentage of certain particles in total counts of particles.

In this case, y-axis was converted from counts to the percentage of certain particle range over the total counts. Figs. 15–17 shows the results after converting the y-axis of Figs. 12–14 respectively. The curves became similar between measurements. The results show the percentages of 2–5 μm particles are over 70% of the total counts, which is dominant at the top in Fig. 15. However, it decreases to around 50% when looking at the bottom with the increase of larger particles. For example, at the top or the middle, the percentage of 7–10 μm particles shows around 20% but it increases to 30% at the bottom, as well as the increase of 15–20 μm and 30–35 μm particles. The results suggest that the particle size distribution may vary at different heights during 1–2 h after stopping the agitation. The percentage of big particles (7–20 μm)

dramatically increase at the bottom height. The particle size segregation could be explained by the mechanism of sedimentation (Krishnamoorthy, 2010), where the top and middle layers are clear and transparent with the finest particles moving inside while the bottom layer is the settling layer where both particles with different size are present. The big particles at the bottom height tend to settle down after a considerable long period. So, considering the particles that can be stably suspended in the liquid, the target particle size could be defined as the finest particles in the clear zone, that is within $2\!-\!7\,\mu m$.

In Fig. 16, the counts of 2–5 μ m particles at the bottom after 10 min firstly soared up to 60% and then decreased to 50% when the probe passing through the liquid from the top. The vertical turbulence might

00:00:00

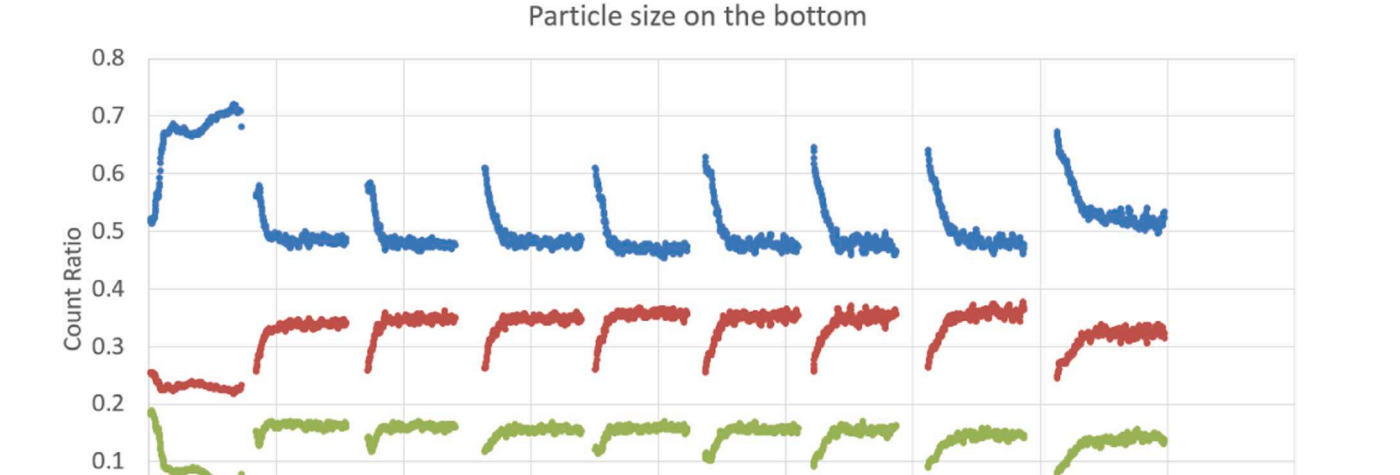
00:14:24

00:28:48

00:43:12

01:55:12

02:09:36



percentage, No Wt, 2-5 (Primary)
 percentage, No Wt, 7-10 (Primary)

Time

01:12:00

01:26:24

01:40:48

00:57:36

percentage, No Wt, 15-20 (Primary)
 percentage, No Wt, 30-35 (Primary)

Fig. 16. Results of FBRM based on ratio at the bottom positions within 2 h.

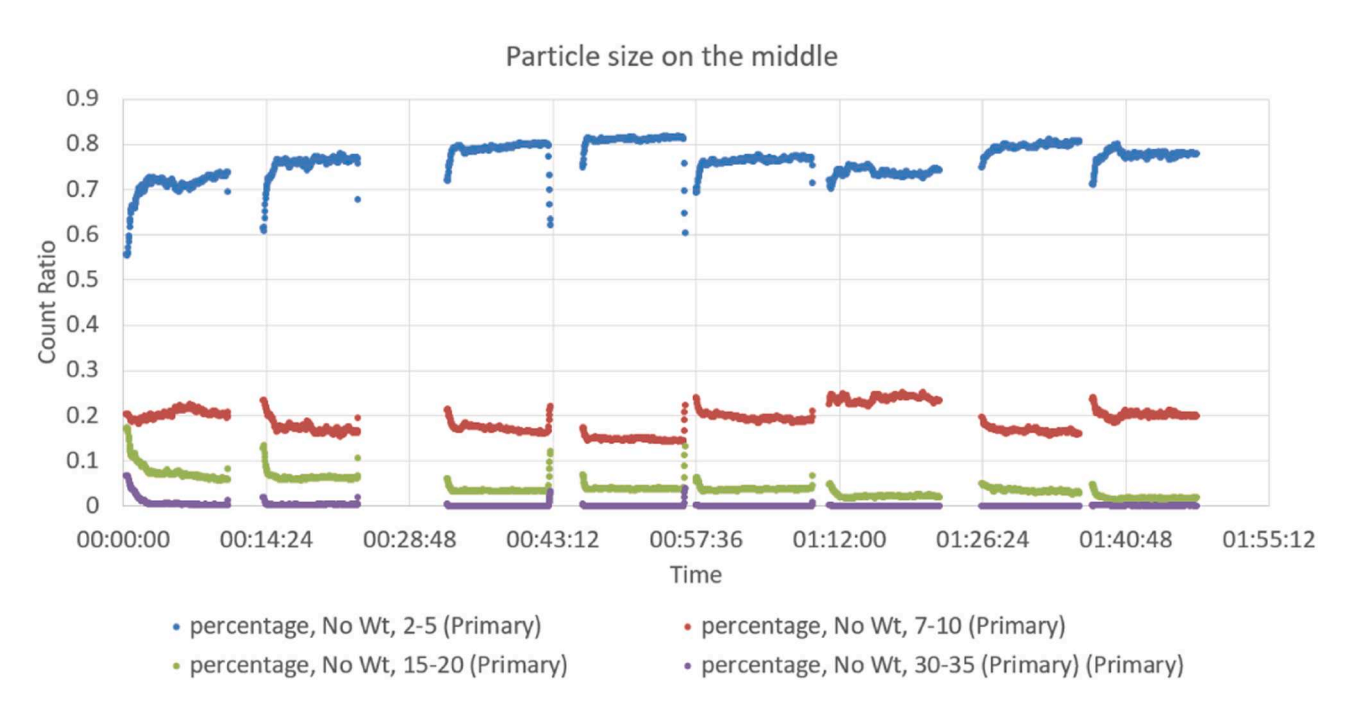


Fig. 17. Results of FBRM based on ratio at the middle within 2 h.

happen inside the liquid when inserting the probe, causing forced convection and particle migration. The turbulence disappeared with time and the number became stable.

3.5. Size distribution of suspended particles for 7 days

The particles within the certain size range could be suspended for 7 days. The three main accumulative percentiles of particle size are calculated and shown in Table 4. The results indicate the particles in the model suspension that can be stably suspended in water for 7 days could be 2–7 $\mu m.$

Based on the results, the particles at the bottom height are larger than the particles moving at the top and middle heights, which is consistent with the results of FBRM. A large amount of big particles settles down and accumulates at the bottom height where the resisting effects became dominant and the counter flow caused by the moving particles would slow down settling velocity of other particles (Govier et al., 1973).

Fig. 18 respectively depicts the particle size distributions (PSDs) of the suspended particles captured at the top from day 1 to day 7 colloids, where the x-axis represents particle diameter and y-axis is the count proportion of particles smaller than x. As shown in the results, the

Table 4 D_{10} , D_{50} , and D_{90} at three different heights in day 1–7 colloids.

Day	Тор			Middle	Middle			Bottom		
	D ₁₀ (μm)	D ₅₀ (μm)	D ₉₀ (μm)	D ₁₀ (μm)	D ₅₀ (μm)	D ₉₀ (μm)	D ₁₀ (μm)	D ₅₀ (μm)	D ₉₀ (μm)	
1	2.3	4.7	6.7	2.0	3.9	6.7	3.6	5.3	7.5	
2	1.7	3.7	6.6	2.4	4.4	7.8	2.3	4.6	7.3	
3	2.2	4.6	6.8	1.6	3.1	5.0	3.0	4.5	6.7	
4	1.9	4.1	7.8	1.7	3.7	5.8	1.6	3.7	6.2	
5	1.6	2.9	5.3	1.8	3.4	5.3	3.8	5.9	8.7	
6	2.2	4.3	6.3	3.4	5.1	7.0	2.8	4.3	6.3	
7	1.7	3.1	5.2	1.6	3.1	5.1	2.6	4.8	7.4	
Mean	1.9 ± 0.1	3.9 ± 0.3	6.4 ± 0.4	2.1 ± 0.3	3.8 ± 0.3	6.1 ± 0.4	$\textbf{2.8} \pm \textbf{0.3}$	4.7 ± 0.3	$\textbf{7.2} \pm \textbf{0.4}$	

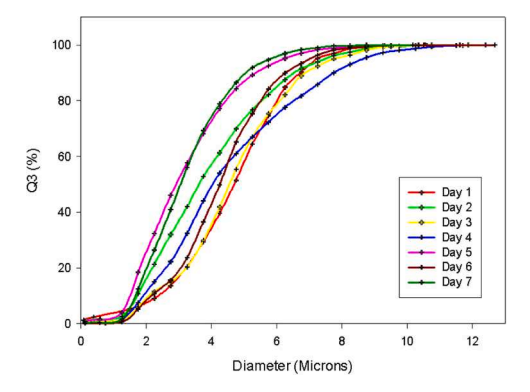


Fig. 18. The cumulative size distribution based on counts from the upper height of day 1–7 colloids.

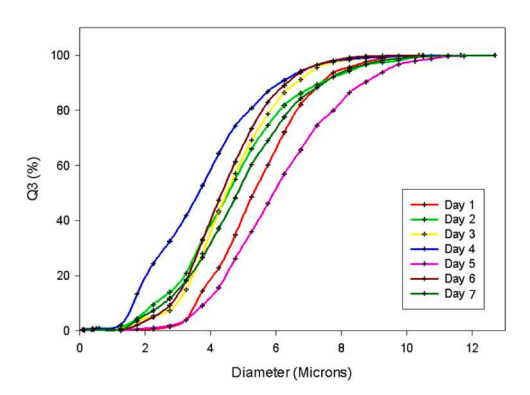


Fig. 19. The cumulative size distribution based on counts from the bottom of day 1–7 colloids.

fraction of the small particulates in the region of 1–4 μm generally increased with time, where the curves from left are day 5, day 7, day 2, day 4, day 6, day 3 and day 1 respectively, indicating the increase percentage of fines (1–4 μm) or decrease of big particles (4–8 μm) in the colloids. Since no new particle was added in the system and breakage was unlikely to happen in the still water without stirring, one possible explanation could be the settling of big particles.

Fig. 19 shows the PSDs at the bottom in 5 colloids respectively. Similar to the upper height, it appears to have a broad size distribution. There is an abnormal increase of particulates in 2 μm region in day 4. For the other six days, the fraction of the small particles (2–4 μm) significantly decreased compared with the top and middle heights and most of particles are distributed within 4–8 μm , which is the largest size range in three different heights. Fig. 20 shows the accumulative PSDs of the particulates suspended at the middle height in day 1–7 colloids. Compared with the PSDs from the top and the bottom, particles at middle height have a narrower distribution. The changes of PSD are not significant between the day 1, day 3, day 4, day 5 and day 7. But the

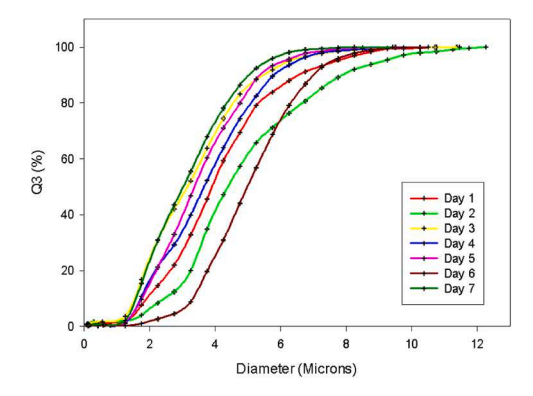


Fig. 20. The cumulative size distribution based on counts from the middle height of day 1-7 colloids.

particles captured from the day 2 and day 6 were obviously larger than the particles from the other four days. For the middle height, a great number of particles are in the range of 2–6 $\mu m.$

4. Conclusion

This work characterized the particle size at different locations of the suspension, including floating, sticking, settling particles and particle suspended at different heights. Three types of sizing techniques are involved and evaluated. It shows that the smallest fraction of particles tends to stick on the wall and stay in the liquid. While, the bigger particles tend to settle down or float on the water surface due to its hydrophobicity. The results also suggest that the size of suspended particles is not uniform and vary at different heights in a suspension after 1 h sedimentation. The particles at the settling zone are generally larger than the particles at the clear and transparent zone. The big particles (7–20 μ m) in settling zone have been excluded. Based on the results, the target size range that could be stably suspended in CaCO3-water system for a long period is successfully defined as 2–7 μ m.

Declaration of Competing Interest

The authors declare that they have no known competing financial interests or personal relationships that could have appeared to influence the work reported in this paper.

References

Bozon, A., Fries, L., Kammerhofer, J., Forny, L., Niederreiter, G., Palzer, S., Salman, A.D., 2022. Effect of heterogeneous hydrophobic coating on floating of insoluble particles. Powder Technol. 395, 592–603.

Zhang, Z.C., Li, Y.P., Zhang, L.J., Chen, D.X., 2023. Drag force modification model for turbulent suspended-load sediment solid–liquid two-phase flow. J. Fluids Struct. 118, 103861.

Kriebitzsch, S.H.L., van der Hoef, M.A., Kuipers, J.A.M., 2013. Drag force in discrete particle models-Continuum scale or single particle scale? AIChE J. 59, 316–324.

- Laxminarsimha Rao, V., Das, S.L., 2015. Drag force on a liquid domain moving inside a membrane sheet surrounded by aqueous medium. J. Fluid Mech. 779, 468–482.
- Gao, Y., et al., 2022. The role of fluid drag force in the dynamic process of two-phase flow-like landslides. Landslides 19, 1791–1805.
- Krishnamoorthy, P., 2010. Sedimentation model and analysis for differential settling of two - particle - size suspensions in the Stokes region. Int. J. Sediment Res. 25, 119–133.
- Govier, G.W., Aziz, K., Schowalter, W.R., 1973. The flow of complex mixtures in pipes. J. Appl. Mech. 40, 404–404.
- Felicetti, M.A., et al., 2009. Influence of particle size, applied compression, and substratum material on particle-surface adhesion force using the centrifuge technique. Ind. Eng. Chem. Res. 48, 877–887.
- Götzinger, M., Peukert, W., 2004. Particle adhesion force distributions on rough surfaces. Langmuir 20, 5298–5303.
- Negreiros, A.A., Althaus, T.O., Niederreiter, G., Palzer, S., Hounslow, M.J., Salman, A.D., 2015. Microscale study of particle agglomeration in oil-based food suspensions: the effect of binding liquid. Powder Technol. 270, 528–536.
- Bian, X., Kim, C., Karniadakis, G.E., 2016. 111 years of Brownian motion. Soft Matter 12, 6331-6346
- Murshed, S.M.S., et al., 2020. Experimental research and development on the natural convection of suspensions of nanoparticles—a comprehensive review. Nanomater. (Basel, Switz.) 10, 1–35.
- Hagiwara, I., Tokuhiro, A., Oduor, P.G., 2014. Natural convection heat transfer of hydrophilic particle suspension: Implications on nuclear waste remediation. Int. J. Heat. Mass Transf. 78, 636–647.
- Sodhi, I., Mallepogu, P., Thorat, V.P., Kashyap, M.C., Sangamwar, A.T., 2019. Insights on role of polymers in precipitation of celecoxib from supersaturated solutions as assessed by focused beam reflectance measurement (FBRM). Eur. J. Pharm. Sci. 137, 104983–104983.

- Kumar, V., Taylor, M.K., Mehrotra, A., Stagner, W.C., 2013. Real-time particle size analysis using focused beam reflectance measurement as a process analytical technology tool for a continuous granulation-drying-milling process. AAPS PharmSciTech 14, 523–530.
- Heath, A., et al., 2002. Estimating average particle size by focused beam reflectance measurement (FBRM). Part. Part. Syst. Charact. 19, 84–95.
- Barrett, P., Glennon, B., 1999. In-line FBRM monitoring of particle size in dilute agitated suspensions. Part. Part. Syst. Charact. 16, 207–211.
- Dave, K., et al., 2018. Feasibility of focused beam reflectance measurement (FBRM) for analysis of pharmaceutical suspensions in preclinical development. AAPS PharmSciTech 19, 155–165.
- Denesuk, M., Smith, G.L., Zelinski, B.J.J., Kreidl, N.J., Uhlmann, D.R., 1993. Capillary penetration of liquid droplets into porous materials. J. Colloid Interface Sci. 158, 114–120.
- Bai, Y., Wall, C., Pham, H., Esker, A., Williams, C.B., 2019. Characterizing binder–powder interaction in binder jetting additive manufacturing via sessile drop goniometry. J. Manuf. Sci. Eng. 141.
- Mitchell, W.R., Forny, L., Althaus, T., Niederreiter, G., Palzer, S., Hounslow, M.J., Salman, A.D., 2020. Tracking of powder lump formation and dispersion with the use of FBRM technology and video recordings. Powder Technol. 367, 10–19.
- Castellanos, A., 2005. The relationship between attractive interparticle forces and bulk behaviour in dry and uncharged fine powders. Adv. Phys. 54, 263–376.
- Likhachev, E.R., 2003. Dependence of water viscosity on temperature and pressure. Tech. Phys. 48, 514–515.
- Pellicer, J., García-Morales, V., Guanter, L., Hernández, M.J., Dolz, M., 2002. On the experimental values of the water surface tension used in some textbooks. Am. J. Phys. 70, 705–709.